

Cdk1-dependent control of membrane-trafficking dynamics

Derek McCusker^{a,b,*}, Anne Royou^{a,b}, Christophe Velours^{a,b}, and Douglas Kellogg^{c,*}

^aEuropean Institute of Chemistry and Biology, 33607 Pessac, France; ^bInstitut de Biochimie et Génétique Cellulaires, Centre National de la Recherche Scientifique, Unité Mixte de Recherche 5095, Université de Bordeaux, F-33000 Bordeaux, France; ^cDepartment of Molecular, Cell and Developmental Biology, University of California, Santa Cruz, Santa Cruz, CA 95064

ABSTRACT Cyclin-dependent kinase 1 (Cdk1) is required for initiation and maintenance of polarized cell growth in budding yeast. Cdk1 activates Rho-family GTPases, which polarize the actin cytoskeleton for delivery of membrane to growth sites via the secretory pathway. Here we investigate whether Cdk1 plays additional roles in the initiation and maintenance of polarized cell growth. We find that inhibition of Cdk1 causes a cell surface growth defect that is as severe as that caused by actin depolymerization. However, unlike actin depolymerization, Cdk1 inhibition does not result in a massive accumulation of intracellular secretory vesicles or their cargoes. Analysis of post-Golgi vesicle dynamics after Cdk1 inhibition demonstrates that exocytic vesicles are rapidly mistargeted away from the growing bud, possibly to the endomembrane/vacuolar system. Inhibition of Cdk1 also causes defects in the organization of endocytic and exocytic zones at the site of growth. Cdk1 thus modulates membrane-trafficking dynamics, which is likely to play an important role in coordinating cell surface growth with cell cycle progression.

Monitoring Editor

Patrick J. Brennwald
University of North Carolina

Received: Oct 5, 2011

Revised: Jun 6, 2012

Accepted: Jun 27, 2012

INTRODUCTION

Oscillations in cyclin-dependent kinase (Cdk) activity drive the core cell cycle events of chromosome duplication and segregation (Nasmyth, 2001). These core events are coordinated with changes in cell polarity and cell growth as cells progress through the cell cycle (Moseley and Nurse, 2009). In budding yeast, a single cyclin-dependent kinase called Cdk1 controls chromosome duplication and segregation, as well as initiation of polarized cell growth that leads to formation of a daughter cell (Culotti and Hartwell, 1971; Lew and Reed, 1993; Moffat and Andrews, 2004). Cdk1 is thus the nexus at which cell growth and cell cycle progression are controlled.

This article was published online ahead of print in MBcC in Press (<http://www.molbiolcell.org/cgi/doi/10.1091/mbc.E11-10-0834>) on July 5, 2012.

*These authors contributed equally to this work.

Address correspondence to: Douglas Kellogg (kellogg@darwin.ucsc.edu), Derek McCusker (mccusker@iecb.u-bordeaux.fr).

Abbreviations used: 1NM-PP1, 4-amino-1-tert-butyl-3-(1'-naphthylmethyl)pyrazolo[3,4-d]pyrimidine; Cdk, cyclin-dependent kinase; GFP, green fluorescent protein; Lat-A, latrunculin-A; PIP2, phosphatidylinositol 4,5-bisphosphate; PMSF, phenylmethylsulfonyl fluoride.

© 2012 McCusker et al. This article is distributed by The American Society for Cell Biology under license from the author(s). Two months after publication it is available to the public under an Attribution–Noncommercial–Share Alike 3.0 Unported Creative Commons License (<http://creativecommons.org/licenses/by-nc-sa/3.0>).

"ASCB®," "The American Society for Cell Biology®," and "Molecular Biology of the Cell®" are registered trademarks of The American Society of Cell Biology.

Polarized cell growth in budding yeast requires coordination of the actin cytoskeleton with membrane-trafficking pathways. The Rho-family GTPases Rho1 and Cdc42 are activated in a Cdk1-dependent manner in a defined patch at the cortex, where they recruit formin proteins to initiate formation of actin cables (Evangelista et al., 1997; Nern and Arkowitz, 2000; Shimada et al., 2000). The actin cables extend radially into the cytoplasm, serving as tracks for myosin motors that deliver post-Golgi vesicles to the plasma membrane (Schott et al., 1999). Vesicles are tethered at the plasma membrane before fusion by the exocyst complex (TerBush and Novick, 1995). Cdc42 and Rho1 interact with specific exocyst subunits in a GTP-dependent manner, which, together with phosphatidylinositol 4,5-bisphosphate (PIP2) binding, is required for polarized growth (Guo et al., 2001; Zhang et al., 2008). These mechanisms direct secretory vesicles carrying components required for cell growth to a defined site of exocytosis on the cell surface.

Endocytosis-associated actin patches are also localized to the site of bud growth and form a ring that surrounds the presumptive bud site (Kilmartin and Adams, 1984; Amberg, 1998; Layton et al., 2011). Localized endocytosis in proximity to sites of exocytosis may optimize cell polarity by recycling polarity determinants that would otherwise diffuse as the membrane grows (Valdez-Taubas and Pelham, 2003; Marco et al., 2007). The mechanisms responsible for

the organization of endocytic and exocytic zones at the site of cell growth are unknown.

Cdk1 is required for polarization of the actin cytoskeleton and phosphorylates key regulators of Rho-family GTPases that direct actin polarization (Knaus *et al.*, 2007; McCusker *et al.*, 2007; Sopko *et al.*, 2007; Kono *et al.*, 2008). Much attention has therefore focused on a role for Cdk1 in initiating cell growth via polarization of the actin cytoskeleton. However, Rho-family GTPases also control endocytic and exocytic trafficking events (Kroschewski *et al.*, 1999; Adamo *et al.*, 2001; Guo *et al.*, 2001; Murray and Johnson, 2001; Wu *et al.*, 2008). Moreover, a systematic mass spectrometry screen for targets of Cdk1 identified many endocytic and exocytic proteins (Holt *et al.*, 2009). We therefore tested whether the role of Cdk1 in the control of polarized cell growth extends beyond its known role in controlling the actin cytoskeleton. To do so, we investigated the dynamics of membrane-trafficking pathways after Cdk1 inhibition.

RESULTS

Inhibition of Cdk1 attenuates cell surface growth to a similar extent as actin depolymerization

We previously discovered that acute Cdk1 inhibition caused rapid attenuation of secretory vesicle delivery to the growing bud, resulting in a block of polar growth (McCusker *et al.*, 2007). These studies used an analogue-sensitive allele of Cdk1 (*cdk1-as1*), which enabled rapid and specific inhibition of Cdk1 activity with the adenine analogue 4-amino-1-*tert*-butyl-3-(1'-naphthylmethyl)pyrazolo[3,4-*d*]pyrimidine (1NM-PP1; Bishop *et al.*, 2001). To investigate how Cdk1 controls polarized cell growth, we compared the effects of *cdk1-as1* inhibition to the effects caused by latrunculin-A (Lat-A), an F-actin poison that causes rapid actin depolymerization and a block in delivery of vesicles to the growing bud (Ayscough *et al.*, 1997). A synchronous population of unbudded *cdk1-as1* cells was obtained by centrifugal elutriation and released into fresh media. On initiation of bud emergence, cells were treated for 1 h with 1NM-PP1, Lat-A, or both 1NM-PP1 and Lat-A (Figure 1A). The mean bud surface area was then calculated and compared with the mean at time zero, which was set to 100% (Figure 1B). In control cells treated with dimethyl sulfoxide (DMSO), buds increased in size by 340%. In contrast, buds in cells treated with 1NM-PP1 or Lat-A increased in size by only 160 and 180%, respectively (Figure 1B). Attenuation of bud growth by *cdk1-as1* inhibition was not due simply to depolarization of growth, because mother cells did not grow after *cdk1-as1* inhibition (Figure 1C). Treatment of wild-type *CDK1* cells with 1NM-PP1 did not attenuate growth (Figure 1D). Inhibition of *cdk1-as1* and F-actin simultaneously did not show strong additive effects. We conclude that the contribution of Cdk1 to polarized growth is comparable to that of F-actin, consistent with Cdk1 making a major contribution to polarized cell surface growth via actin-dependent processes.

Cdk1 activity does not contribute to polarized cell growth solely via modulation of the actin cytoskeleton

Actin depolymerization results in accumulation of post-Golgi vesicles due to a failure in vesicle delivery to the growing bud (Novick and Botstein, 1985). Actin depolymerization also blocks endocytosis (Kubler and Riezman, 1993). If Cdk1 is primarily required for polarization of the actin cytoskeleton to deliver vesicles, inhibition of *cdk1-as1* could result in post-Golgi vesicle accumulation and an endocytic block. To test this, we first visualized a green fluorescent protein (GFP)-tagged version of Sec4, which is a Rab-GTPase component of post-Golgi secretory vesicles that was previously used as a post-Golgi vesicle marker (Schott *et al.*, 2002). Actin was visual-

ized in the same cells by rhodamine-phalloidin staining, enabling imaging of endocytosis-associated actin patches and actin cables (Kilmartin and Adams, 1984). Deconvolved optical sections of asynchronously growing cells were projected to observe GFP-Sec4 particles and actin structures in the cell (Figure 2A and Supplemental Figures S1 and S2).

In control cells, GFP-Sec4 localized to growth sites and to a few cytoplasmic particles, as previously reported (Figure 2A and Supplemental Figure S1; Schott *et al.*, 2002). On Lat-A treatment, actin structures disappeared and many GFP-Sec4 particles accumulated in the cytoplasm, as expected for accumulation of secretory vesicles (Figure 2A and Supplemental Figures S1 and S2). In contrast, treatment of *cdk1-as1* cells with 1NM-PP1 did not cause accumulation of GFP-Sec4 particles. Instead, GFP-Sec4 was observed as a diffuse cytoplasmic signal and in a few particles (Figure 2A and Supplemental Figure S1). Actin patches lost their polarized organization, and actin cables became disorganized (Figure 2A and Supplemental Figure S2; McCusker *et al.*, 2007). Fewer cables were observed, and those that were visible were short and failed to orient along the mother-daughter axis (Supplemental Figure S2, arrows). Of importance, GFP-Sec4 localized normally to the bud neck in neighboring large-budded cells that had presumably undergone anaphase before inhibition of *cdk1-as1* (Figure 2A, arrow). This demonstrated that inhibition of *cdk1-as1* had specific effects on post-Golgi vesicles involved in polarized growth, since membrane addition at the site of cell division is Cdk1-independent in budding yeast and sea urchins (Shuster and Burgess, 2002; VerPlank and Li, 2005).

The failure to accumulate post-Golgi vesicles after inhibition of *cdk1-as1* could be due to a failure to generate the vesicles. In this case, treatment of *cdk1-as1* cells with 1NM-PP1 and Lat-A simultaneously should not lead to vesicle accumulation. However, we found that GFP-Sec4 particles accumulated to the same extent when *cdk1-as1* cells were treated with Lat-A and 1NM-PP1 together as when cells were treated with Lat-A alone (Figure 2A and Supplemental Figure S1). We conclude that Cdk1 activity is not required for bulk post-Golgi vesicle production. Together these observations demonstrate that depolymerization of actin or inhibition of Cdk1 has fundamentally different effects on accumulation of post-Golgi vesicles, implying that Cdk1 does not act simply to generate and maintain a polarized actin cytoskeleton for delivery of vesicles to the growing bud.

Cdk1 is required for maintaining discrete zones of endocytosis and exocytosis at the site of polarized cell growth

Control cells showed a striking segregation of exocytic and endocytic compartments, as revealed by GFP-Sec4 or Sec2-GFP and actin staining (Figure 2, A, top, and B). Before bud emergence, a belt of endocytosis-associated actin patches surrounded a central zone of exocytosis, which was evident from views looking down at the polarized surface of the cell (Figure 2B). GFP-Sec4 remained polarized at the bud tip until after chromosome segregation, when it relocated to the bud neck (Figure 2A). Previous work found that actin patches form a ring at the site of bud growth, and other studies found that exocytic proteins form a tightly focused spot (Kilmartin and Adams, 1984; Amberg, 1998; Finger *et al.*, 1998; Layton *et al.*, 2011). The merged image in Figure 2B shows the localization of endocytic and exocytic zones in the same cell, which emphasizes the interesting organization of these processes at the site of cell growth. Inhibition of *cdk1-as1* eliminated the distinct zones of endocytosis and exocytosis (Figure 2A and Supplemental Figures S1 and S2).

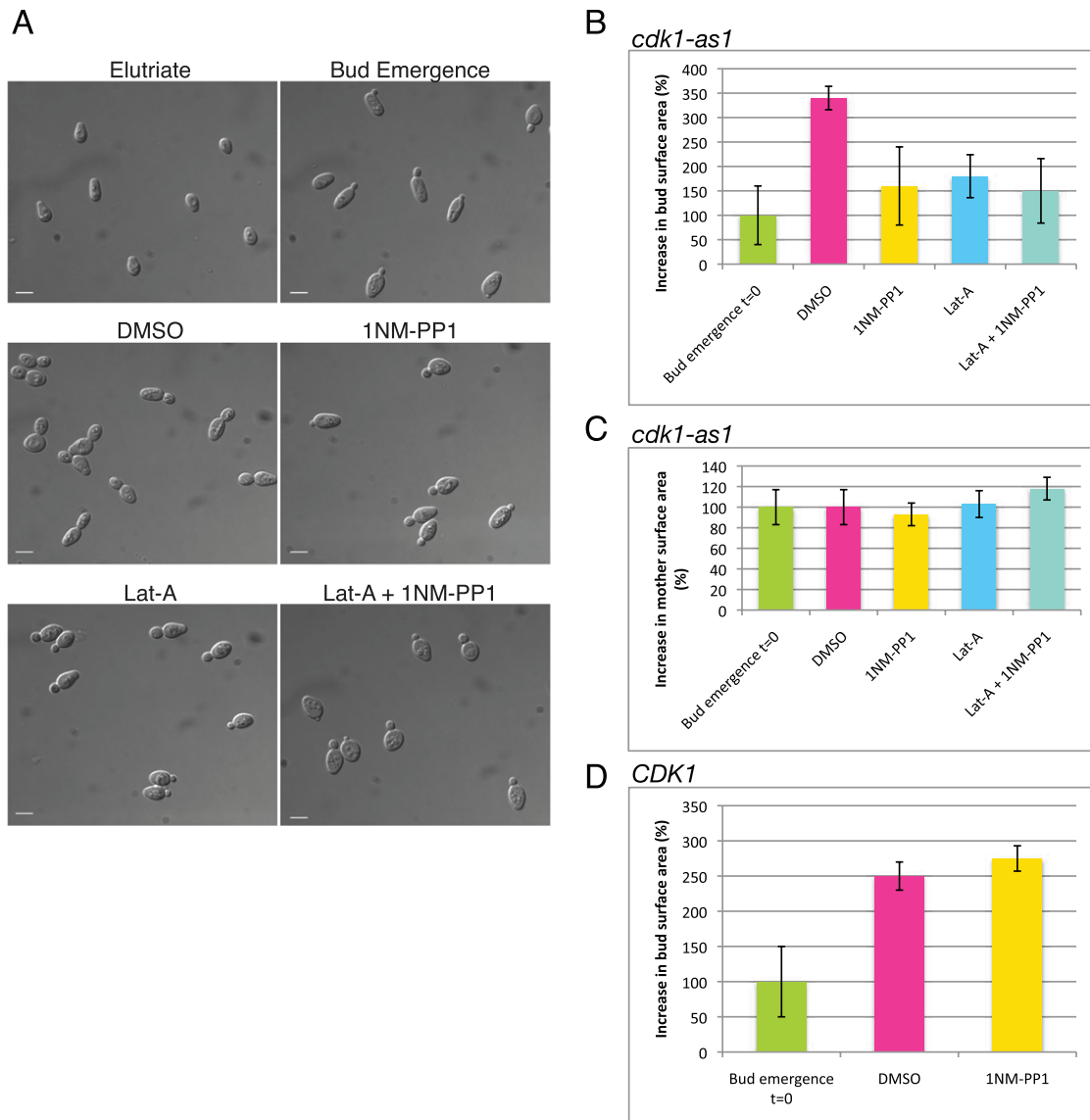


FIGURE 1: Inhibition of Cdk1 attenuates bud growth as severely as actin depolymerization. (A) Images showing representative samples of cells. Elutriate: cells immediately after elutriation; Bud Emergence: cells at the time when inhibitors were added. Cells were treated for 1 h with DMSO as a control or with the indicated inhibitors. Scale bar, 5 μm . (B) Quantitation of the surface area of buds in *cdk1-as1* cells 1 h after treatment. The bar labeled $t = 0$ shows the size of buds at the time of inhibitor addition. Absolute bud size at $t = 0$ was 5 μm^2 . (C) Quantitation of mother cell surface area in *cdk1-as1* cells treated with inhibitors. Absolute mother size at $t = 0$ was 29 μm^2 . (D) Quantitation of bud growth in wild-type cells treated with 1NM-PP1 for 1 h. Absolute bud size at $t = 0$ was 4 μm^2 . Error bars show mean \pm SD, where n is at least 100 cells.

Cdk1 is not required for endocytosis

The defects in post-Golgi vesicle accumulation and localization caused by *cdk1-as1* inhibition could reflect defects in a membrane-trafficking pathway. We therefore tested whether *cdk1-as1* activity is required for normal membrane-trafficking events in the endocytic and exocytic pathways. We first tested whether inhibition of *cdk1-as1* caused defects in endocytosis. Wild-type *CDK1* or *cdk1-as* cells were treated with 1NM-PP1 for 1 h. Cells were placed on ice to block endocytosis and then pulsed with the lipophilic dye FM4-64 (Vida and Emr, 1995). After washing away excess dye, we released cells at 25°C to initiate endocytic uptake of the dye (Figure 3A). Imaging cells periodically during the pulse chase provided a means of assaying the function of the endocytic pathway after *cdk1-as1* inhibition (Figure 3B). In wild-type *CDK1* cells, FM4-64

was endocytosed and over time was chased through the endocytic system, where it terminally labeled the vacuole. After 12 min, FM4-64 could be visualized in punctate perivacuolar structures in both wild-type *CDK1* and *cdk1-as1* cells treated with 1NM-PP1. These structures most likely correspond to the prevacuolar compartment. By 16 min, FM4-64 had reached the limiting membrane of the vacuole in both *CDK1* and *cdk1-as1* cells treated with 1NM-PP1. To ensure that our pulse-chase assay was sufficiently sensitive to detect defects in endocytosis, we used the endocytosis-defective *sla2 Δ* mutant as a control (Holtzman *et al.*, 1993). In this mutant, persistent plasma membrane staining reflected defective internalization of the dye, and in many cells, bright fluorescent puncta formed as dye accumulated in an early endosomal compartment, as reported previously (Kim *et al.*, 2006). Because the kinetics of

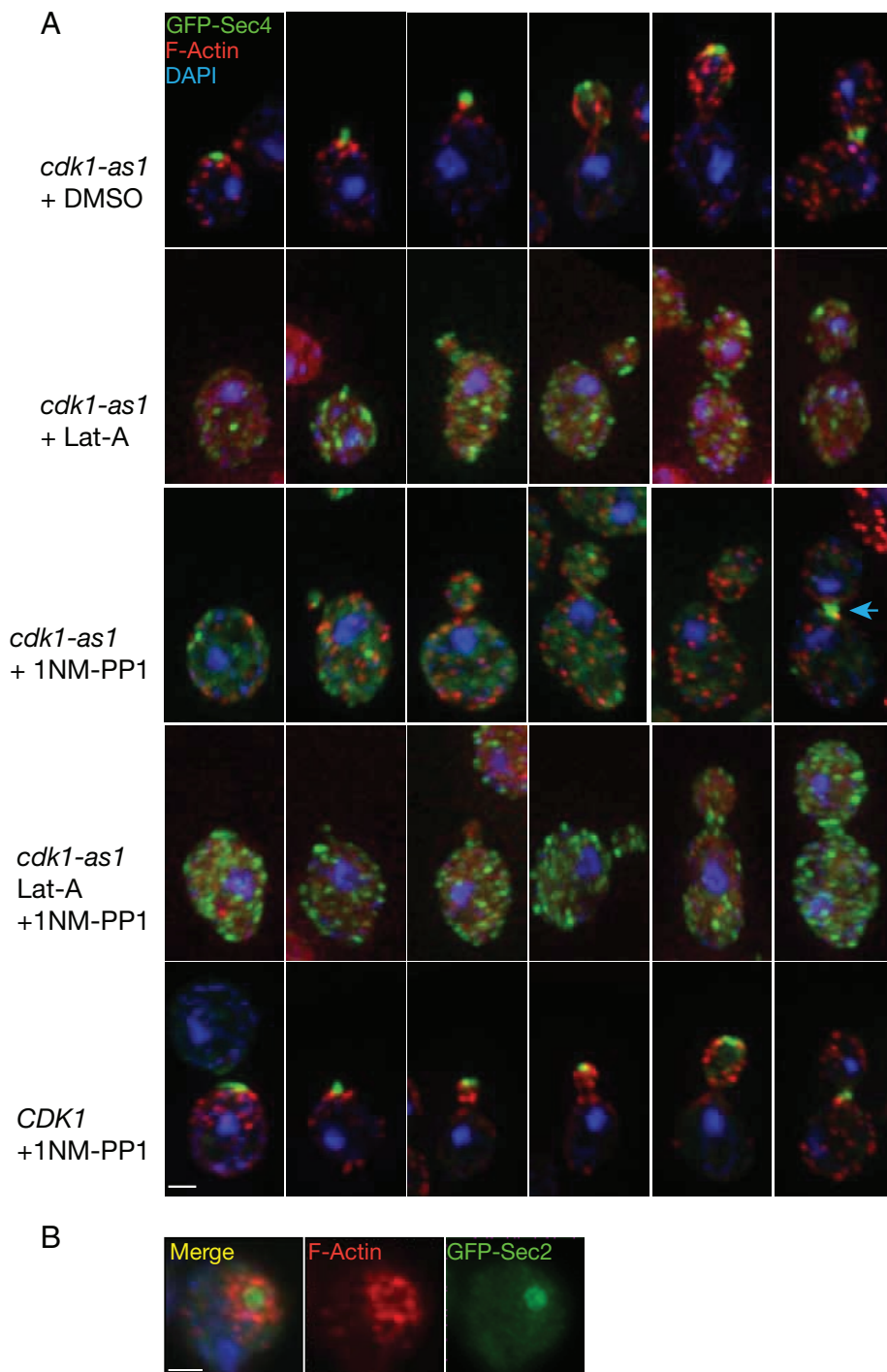


FIGURE 2: Behavior of GFP-Sec4 and actin after inhibition of Cdk1. (A) Asynchronous cells were treated for 1 h with DMSO or with the indicated inhibitors and were then fixed and stained. Images show maximum projections of 15–20 deconvolved z-sections through different cells at distinct cell cycle stages. GFP-Sec4 is shown in green, rhodamine-phalloidin in red, and DNA in blue. An arrow denotes the Cdk1-independent localization of GFP-Sec4 to the bud neck postanaphase. Scale bar, 2 μ m. (B) Wide-field fluorescence images showing the top view of an unbudded cell initiating polarization of Sec2-GFP (green), F-actin (red), and DNA (blue). Scale bar, 2 μ m.

FM4-64 internalization was not dramatically impaired after *cdk1-as1* inhibition, we conclude that endocytosis and subsequent transport to the vacuole occur efficiently after *cdk1-as1* inhibition, despite defects in polarized growth.

Endocytosis is not required for secretion in budding yeast (Raths *et al.*, 1993). Thus the accumulation of vesicles in cells treated with Lat-A, but not in *cdk1-as1* cells treated with 1NM-PP1, cannot be explained by a model in which endocytic recycling of proteins needed for secretion continues after Cdk1 inhibition but not after Lat-A treatment.

Cdk1 is not required for transport from the endoplasmic reticulum to the vacuole

We next assayed the pathway that transports carboxypeptidase Y (CPY) from the endoplasmic reticulum (ER) to the vacuole via the Golgi (Hasilik and Tanner, 1978; Stevens *et al.*, 1982). CPY is synthesized in the ER as a 67-kDa proenzyme (p1), which traffics to the Golgi, where it is glycosylated to yield a 69-kDa form (p2; Hasilik and Tanner, 1978). CPY is then routed to the vacuole, where it is cleaved to produce a mature (m) protease (Stevens *et al.*, 1982). Wild-type *CDK1* or *cdk1-as1* cells were treated with DMSO or 1NM-PP1, and CPY transport kinetics were analyzed by pulse-chase and immunoprecipitation (Figure 4A). Inhibition of *cdk1-as1* had no detectable effects on CPY processing. In an additional assay, we found that GFP-tagged carboxypeptidase S (GFP-CPS) was also efficiently targeted to the vacuole after *cdk1-as1* inhibition (Supplemental Figure S3A). Immunoblotting revealed no difference in the levels of GFP-CPS after *cdk1-as1* inhibition (Supplemental Figure S3B). Together these observations demonstrate that Cdk1 activity is not required for transport between the ER and Golgi, between the Golgi and the vacuole, or between endosomes and the vacuole. Of importance, these results also indicate that 1NM-PP1 did not cause nonspecific effects that completely disabled the secretory pathway.

Inhibition of Cdk1 does not result in accumulation of post-Golgi vesicle cargo proteins

We next tested whether Cdk1 inhibition caused defects in transport from the Golgi to the plasma membrane. In budding yeast, secreted proteins exit the Golgi in at least two classes of vesicles. The cell wall β -glucanase Bgl2 is transported directly from the Golgi to the plasma membrane, and another class of vesicles transports invertase, encoded by the *SUC2* gene, to the plasma membrane via an endosomal compartment (Harsay and Schekman, 2002). We monitored trafficking of Bgl2 using an antibody against the protein and Suc2 using a hemagglutinin (HA)-tagged version of the protein that had been used previously (Wiederkehr *et al.*, 2003; Gillingham *et al.*, 2006). *CDK1* or *cdk1-as1*

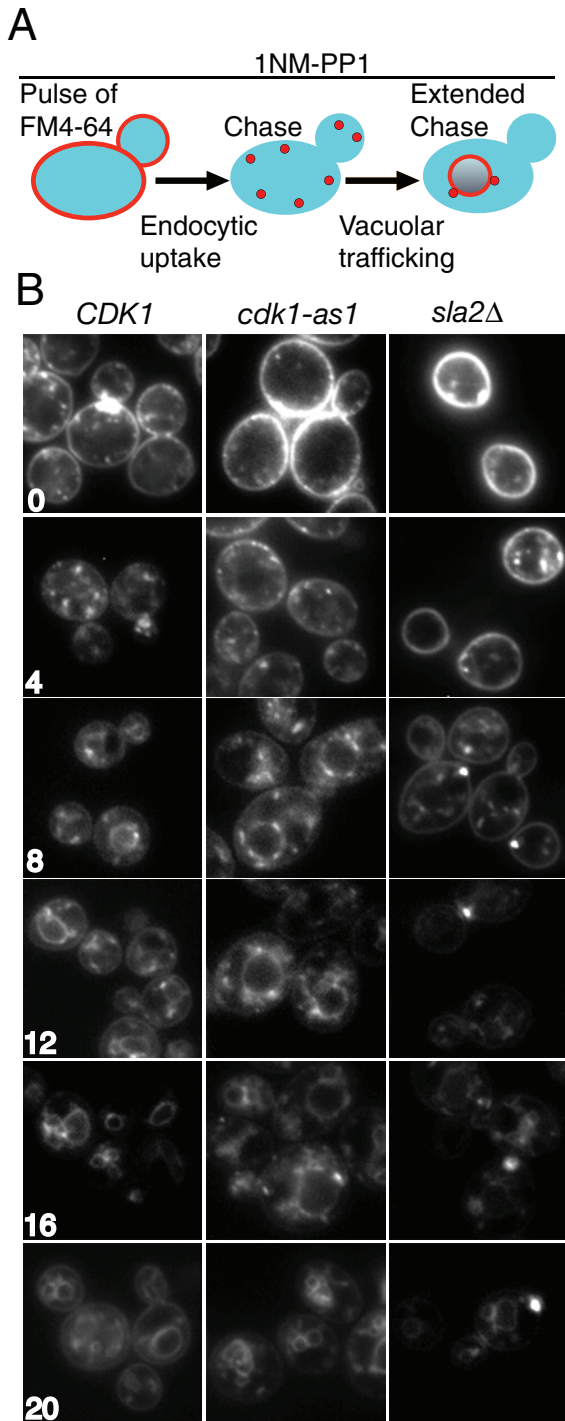


FIGURE 3: Cdk1 activity is not required for endocytosis. (A) Schematic representation of the experiment. *CDK1* and *cdk1-as1* cells were treated for 1 h with 1NM-PP1 and compared with an endocytosis-defective *sla2Δ* control in the following experiment: endocytosis was blocked by placing cells on ice, then a pulse of the lipophilic dye FM4-64 was provided, followed by a chase period in the absence of dye. During the chase, the dye is internalized by endocytosis, transits the endocytic pathway, and is delivered to the vacuole in the presence of 1NM-PP1. (B) Wide-field fluorescence images showing FM4-64 staining in live cells. Numbers indicate the time, in minutes, after initiation of the chase. In the endocytosis-defective *sla2Δ* mutant, FM4-64 accumulates in punctate intracellular structures, and the kinetics of its delivery to the vacuole is delayed.

cells were treated with DMSO or 1NM-PP1 and processed to yield intracellular and extracellular fractions that were probed by Western blotting to assay levels of Bgl2 (Figure 4B) or Suc2 (Figure 4C). As a control, trafficking of Bgl2 and Suc2 were also assayed in cells carrying the *sec6-4* temperature-sensitive mutant. Sec6 is a component of the exocyst complex, which is required for vesicle tethering and fusion at the plasma membrane (TerBush *et al.*, 1996). Thus inactivation of Sec6 causes a rapid block of exocytosis and accumulation of post-Golgi secretory vesicles.

Blocking post-Golgi secretion with the *sec6-4* mutant led to an intracellular accumulation of both Bgl2 and Suc2, as expected (Figure 4, B and C; Adamo *et al.*, 2001). In contrast, intracellular levels of Bgl2 or Suc2 did not increase after *cdk1-as1* inhibition, and instead Suc2 levels appeared to drop slightly (Figure 4, B and C). The failure to accumulate intracellular post-Golgi vesicle cargoes after *cdk1-as1* inhibition contrasted with the effect of actin depolymerization, which caused a moderate accumulation (Figure 4D). This is concordant with earlier work demonstrating that although the actin cytoskeleton is required for polarized growth, it is only partially required for secretion of Suc2 (Novick and Botstein, 1985). Cell viability was not reduced after 1 h of *cdk1-as1* inhibition, making it unlikely that cell death accounted for the lack of cargo accumulation (Supplemental Figure S4). These observations further support the conclusion that inhibition of 1NM-PP1 does not lead to an accumulation of post-Golgi secretory vesicles.

Cdk1 activity is required for normal trafficking of post-Golgi secretory vesicles

To learn more about the fate of post-Golgi vesicles after *cdk1-as1* inhibition, we studied the dynamics of post-Golgi vesicle markers in live cells. *CDK1* and *cdk1-as1* cells were pulse chased with FM4-64 to label the vacuole and treated with 1NM-PP1 or DMSO. Post-Golgi vesicle dynamics were then monitored 1 h after treatment by imaging GFP-Sec4. In *cdk1-as1* cells treated with DMSO and in wild-type *CDK1* cells treated with 1NM-PP1, GFP-Sec4 particles were rapidly transported to the bud. Kymographs were generated to analyze GFP-Sec4 dynamics, revealing that under these imaging conditions, particles were transported at a rate of around 1.7 $\mu\text{m/s}$ (Figure 5A and Supplemental Movies S1–S4). GFP-Sec4 particles often dwelt at the bud neck, presumably reflecting either a time lag before association of the vesicle with an actin cable or the presence of a septin-dependent barrier (Takizawa *et al.*, 2000; Supplemental Movies S1 and S3). A subset of GFP-Sec4 particles cycled between the plasma membrane and the cytoplasm at the end of the mother cell opposite the bud. To our knowledge, the existence of this trafficking behavior has not previously been reported.

Inhibition of *cdk1-as1* severely disrupted the dynamics of GFP-Sec4 trafficking. Few GFP-Sec4 particles were visible, and those that were visible either made short, retrograde movements away from the bud before disappearing or completely failed to move and then often disappeared (Figure 5A and Supplemental Movie S4). GFP-Sec4 disappearance coincided with endomembrane/vacuole localization, suggesting that some vesicles may be consumed in the endomembrane/vacuole (Figure 5A and Supplemental Movie S4). Quantitation of 200–600 particle movements revealed that >55% of GFP-Sec4 particles showed anterograde movements in wild-type *CDK1* cells treated with 1NM-PP1. In contrast, <10% of GFP-Sec4 particles were transported in this manner in *cdk1-as1* cells treated with 1NM-PP1, and many particles disappeared during analysis, which may be due to their targeting to the vacuole (Figure 5B). Western blotting revealed that GFP-Sec4 levels were unchanged after *cdk1-as1* inhibition (Figure 5C). Unlike *cdk1-as1* inhibition,

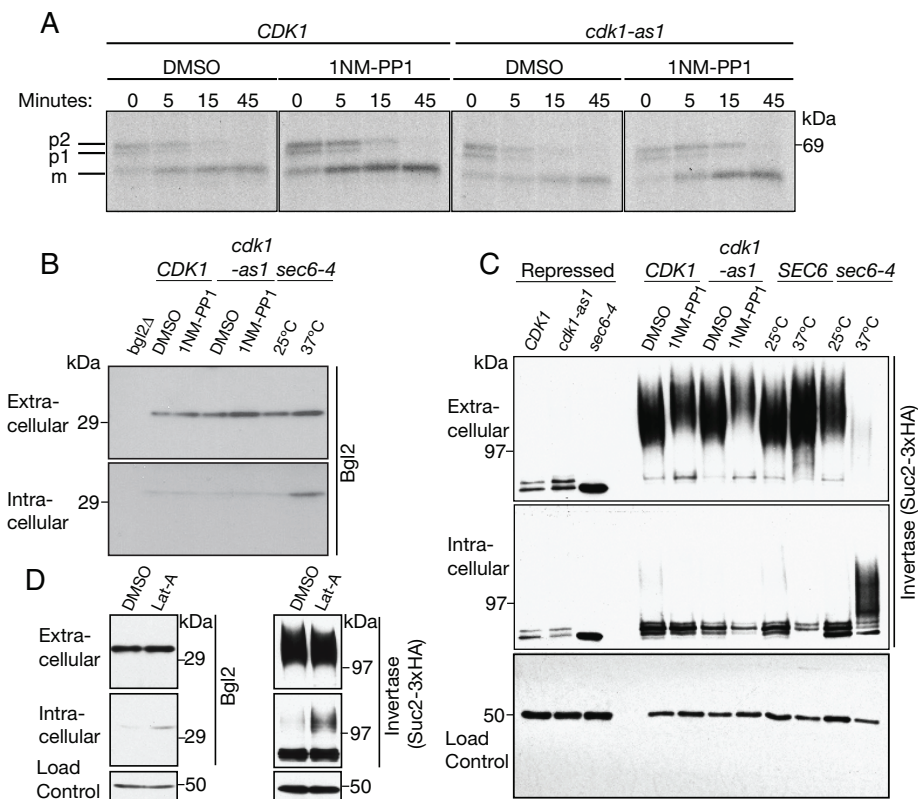


FIGURE 4: Cdk1 inhibition does not result in the intracellular accumulation of post-Golgi vesicle cargoes. (A) *CDK1* and *cdk1-as1* cells were treated with 1NM-PP1 or DMSO control. Cells were then pulsed with ^{35}S -methionine for 10 min and chased for the times indicated. CPY was immunoprecipitated and analyzed by SDS-PAGE. (B) Immunoblot analysis of the extracellular and intracellular pools of the post-Golgi vesicle cargo protein Bgl2. Note that inactivation of *sec6-4* caused an increase in intracellular levels of Bgl2. Nap1 was used as a loading control (not shown). (C) Immunoblot analysis of the extracellular and intracellular levels of Suc2-3xHA. Cells were grown in 2% glucose containing 1NM-PP1 or DMSO control for 1 h. Suc2-3xHA was then induced by shifting cells to 0.1% glucose in the presence of 1NM-PP1 or DMSO and harvesting cells after an additional hour. Note that inactivation of *sec6-4* caused a complete block in secretion of Suc2-3xHA. Nap1 was used as a loading control. (D) Immunoblot analysis of the secreted and intracellular pools of Bgl2 and Suc2-3xHA levels after actin depolymerization for 1 h using latrunculin-A. Nap1 was used as a loading control. Note that the data presented in C and D were obtained in separate experiments.

treatment with Lat-A led to the accumulation of post-Golgi particles in the cytoplasm that did not disappear during analysis (Figure 5A and Supplemental Movie S2). These results indicate that Cdk1 activity is critical for the polarized anterograde trafficking of post-Golgi vesicles and that the effects of inhibition of Cdk1 are distinct from those of actin depolymerization.

The technical challenge of following particles that move at high speeds in an x, y, z-axis is formidable, and it is not possible to image all particles at all times as one would ideally wish. Therefore, we also observed the fate of post-Golgi particles in cells with small buds, which minimized the concern that vesicles were moving out of the focal plane, since the z axis is greatly reduced. These experiments were carried out using a total internal reflection (TIRF) imaging system equipped with a sensitive electron-multiplying charge-coupled device (EM-CCD) camera, which enabled image acquisition at speeds of up to 30 ms. The improved sensitivity of this system facilitated longer observations of GFP-Sec4 dynamics after inhibition of *cdk1-as1*. Consistent with the results presented in Figure 5, kymographs of GFP-Sec4 dynamics 20 min after *cdk1-as1* inhibition revealed a stream-like flow of GFP-Sec4 particles out of the bud and

into the mother cell (Figure 6A). Some of these particles disappeared upon reaching the vacuole membrane (Figure 6C). These observations suggest that all vesicles are not fusing with the plasma membrane in or near the bud after *cdk1-as1* inhibition.

When *cdk1-as1* was inhibited, those particles that moved did so in a vectorial manner at a similar velocity, consistent with motor-mediated transport of post-Golgi vesicles along actin cables. The velocities of vesicle movement in the four vesicle tracks shown in Figure 6A were calculated from the kymographs and found to be 2.6, 2.7, 2.7, and 3.5 $\mu\text{m/s}$, which is within the range of velocity previously reported for myosin motor-mediated transport (Schott *et al.*, 2002). The speed is slightly faster than that of the vesicles shown in Figure 5. This may reflect the fact that the cells in Figure 5 were treated with inhibitor for 1 h before imaging, whereas the cells shown in Figure 6 were treated for 20 min. The movement of vesicles out of the bud after *cdk1-as1* inhibition contrasted with control *CDK1* cells treated with 1NM-PP1, where GFP-Sec4 particles moved from the mother to the bud, as expected (Figure 6B).

Previous work found that the *myo2-66* temperature-sensitive allele caused accumulation of vesicles without causing accumulation of secretory cargoes (Govindan *et al.*, 1995). *MYO2* encodes the myosin that moves vesicles along actin tracks to the bud (Johnston *et al.*, 1991). The failure to accumulate secretory cargoes in *myo2-66* cells is similar to the effects of inhibiting *cdk1-as1*. We therefore considered the possibility that inhibition of *cdk1-as1* blocks Myo2 function and causes accumulation of a class of vesicles that cannot be detected with GFP-Sec4. In previous work, we did not observe accumula-

tion of vesicles by electron microscopy after inhibition of *cdk1-as1* (McCusker *et al.*, 2007). To ensure that our imaging methods can detect the class of vesicles that accumulate in *myo2-66* cells, we repeated the electron microscopy analysis and included a *myo2-66* control. We found that *myo2-66* cells accumulated vesicles, whereas *cdk1-as1* cells treated with 1NM-PP1 did not, which argues against the possibility that inhibition of *cdk1-as1* blocks Myo2 function (Figure 7). In this experiment, we also tested whether *pep4 Δ* , which inactivates a major vacuolar degradation pathway, allowed accumulation of vesicles in *cdk1-as1* cells. We reasoned that *pep4 Δ* could block consumption of vesicles by the vacuole; however, we observed that the effects of inhibiting *cdk1-as1* in *pep4 Δ* cells were no different from the effects that we previously observed of inhibiting *cdk1-as1* in an otherwise wild-type background (Figure 7; McCusker *et al.*, 2007).

We also considered the possibility that the effects of inactivating *cdk1-as1* are due solely to depolarization of the actin cytoskeleton. In this case, the effects of *cdk1-as1* inhibition ought to resemble the effects of a *cdc42* mutant, in which actin filaments are depolarized and disorganized (Adams *et al.*, 1990). To test this, we monitored GFP-Sec4 and endocytosis-associated actin patch

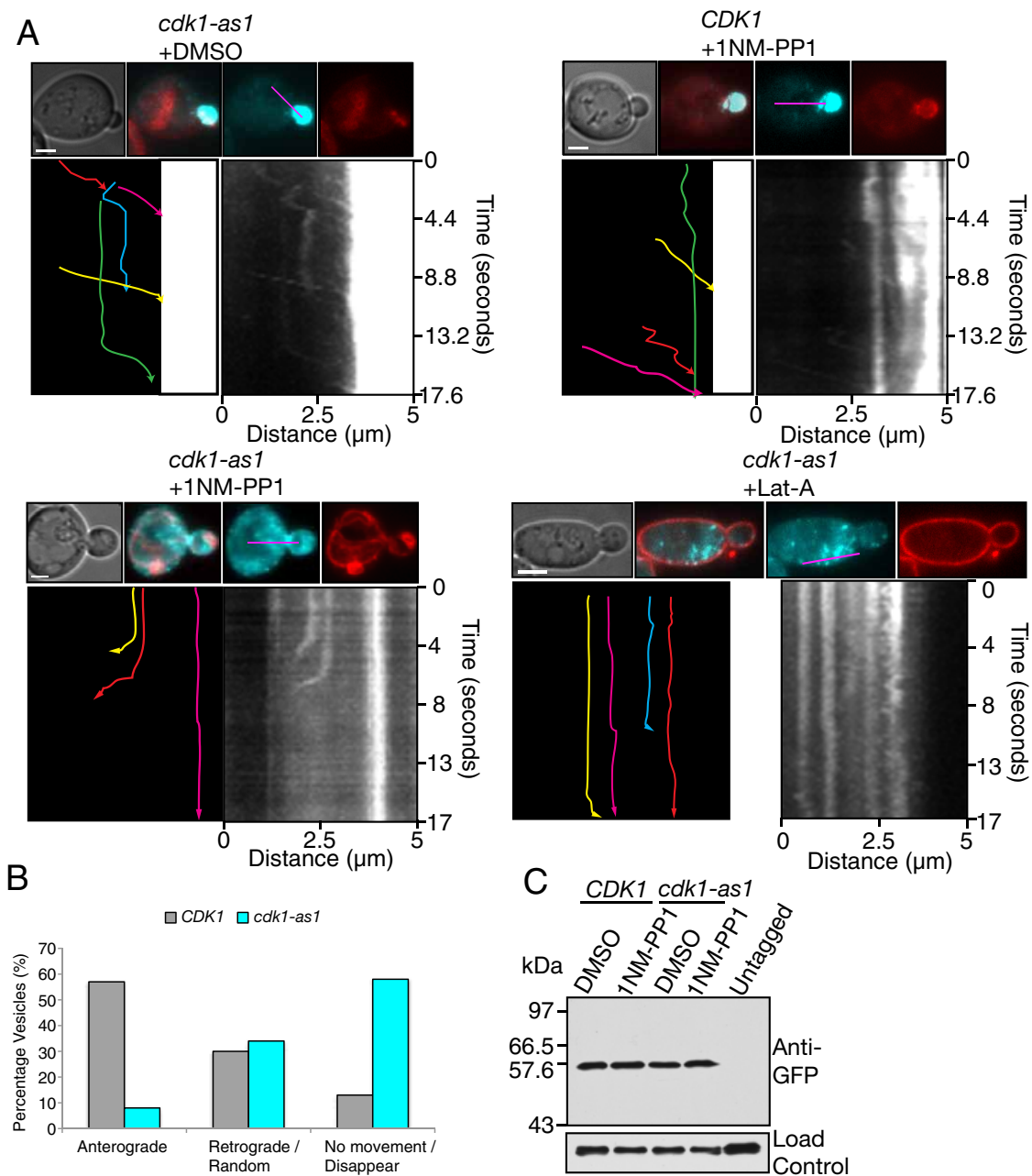


FIGURE 5: Cdk1 inhibition results in aberrant targeting of post-Golgi vesicles. (A) Cells of the indicated genotypes were treated with 1NM-PP1 or Lat-A for 1 h and pulse chased with FM4-64 to label the vacuole. From 80 to 100 images were then acquired at 220-ms intervals and stacked vertically to generate kymographs. In each set, shown at the top are a differential interference contrast image, merged images of GFP-Sec4 (cyan) and FM4-64 (red), and the individual images used to generate the merge. The longitudinal line used to generate kymographs is shown in purple. Lower right, the resulting kymograph; lower left, a tracing of the kymograph in which each colored line represents the trajectory of a different GFP-Sec4 particle, with the arrowhead showing the direction of movement. Scale bar, 2 μm . (B) Quantitation of vesicle behavior. $n = 282$ vesicles for CDK1 and $n = 671$ vesicles for *cdk1-as1*. (C) Levels of GFP-Sec4 after 1 h of treatment with 1NM-PP1 or DMSO. Nap1 was used as a loading control.

localization in wild-type and *cdc42-1* cells. In the *cdc42-1* cells at the restrictive temperature, cells arrested with no buds and depolarized actin patches, as previously reported, and GFP-Sec4 particles accumulated (Figure 8). These results are consistent with previous work on Igq1, which interacts with Cdc42 and is required for normal polarization of the actin cytoskeleton. Like *cdc42* mutants, deletion of the *IQG1* gene causes a loss of polarity pheno-

type, as well as accumulation of vesicles that can be seen by electron microscopy (Osman and Cerione, 1998). Actin mutants that cause disorganization of the actin cytoskeleton also cause accumulation of vesicles (Novick and Botstein, 1985). Together these results indicate that *cdk1-as1* inhibition results in a defect that is distinct from that produced by actin depolymerization or actin depolarization.

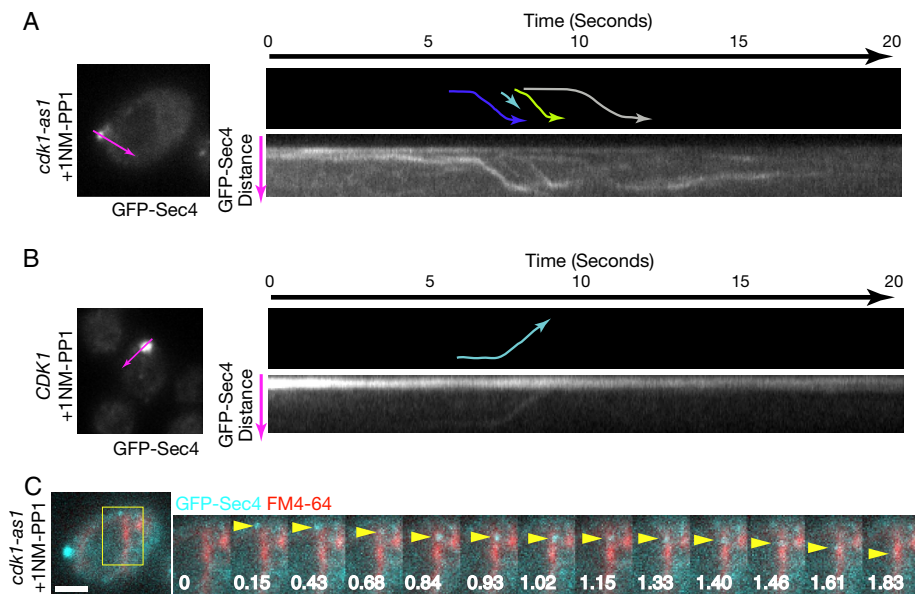


FIGURE 6: Retrograde streaming of post-Golgi particles from sites of polarized growth into the mother cell after *cdk1-as1* inhibition. (A) *cdk1-as1* cells or (B) *CDK1* cells were treated with 1NM-PP1 for 20 min and imaged. Approximately 650 images were acquired at 30-ms intervals and stacked vertically to generate kymographs. In each set of images, shown at the top is a schematic representation of the kymograph in which the colored lines indicate individual particle trajectories and the arrow indicates the direction of movement. The longitudinal line used to generate kymographs is shown in purple on an image of the cell used for imaging. (C) A series of images from the *cdk1-as1* cell shown in A, where a GFP-Sec4 particle (indicated by a yellow arrowhead) moves to the vacuolar membrane (shown in red after staining with FM4-64) and then disappears. Time is shown in seconds. Scale bar, 2 μ m.

DISCUSSION

We propose that Cdk1 controls membrane trafficking events that are required for proper delivery of vesicles to the cell surface during polarized growth. A recent proteomics study identified many components of the secretory pathway as potential direct targets of Cdk1, consistent with a role for Cdk1 in controlling membrane-trafficking events (Holt et al., 2009).

The events controlled by Cdk1 that are required for normal membrane trafficking are unknown. One possibility is that Cdk1 directs post-Golgi vesicles to the site of polarized growth. It could do this by initiating events that mark vesicles with a targeting signal or by activating a docking site at the site of cell growth. In the absence of the targeting signals, vesicles could be redirected to the endomembrane system or vacuole via a default trafficking pathway. Previous studies found that the vacuole may be the default trafficking destination in the yeast secretory pathway and that additional targeting or retention signals exist for sorting to other destinations (Roberts et al., 1992; Wilcox et al., 1992). Alternatively, Cdk1 could be required to suppress signals that target post-Golgi vesicles to the endomembrane system or vacuole. Additional models are possible, and further work will be necessary to fully understand the molecular mechanisms underlying the effects of Cdk1 on membrane traffic during growth of the daughter cell membrane.

Disappearance of vesicles after Cdk1 inhibition was dependent upon actin filaments. Previous work found that Cdc42 stimulates actin polymerization at the vacuole, and Cdc42 and Rho1 localize to the vacuole membrane, where they regulate actin-dependent membrane fusion events (Eitzen et al., 2001; Isgandarova et al., 2007). Thus actin filaments associated with the vacuole or endomembrane system could be responsible for movement of vesicles toward these compartments, where they could be consumed via a Rho-GTPase-

dependent mechanism. This model would be consistent with our observation that disappearance of vesicles in vivo appears to occur near the endomembrane system.

Although our results suggest that vesicles are redirected to the endomembrane system or vacuole, we cannot rule out other fates. For example it is possible that vesicles are redirected to the Golgi or that the vesicles are dismantled via a novel mechanism.

Several observations suggest that the effects of *cdk1-as1* inhibition are not due to depolarization of the actin cytoskeleton. First, the effects of *cdk1-as1* inhibition are different from the effects of inactivating Cdc42, which is required for actin polarization. Inhibition of *cdk1-as1* with the concentrations of 1NM-PP1 used here results in rapid cessation of bud growth, and the mother cell does not increase in volume (Bishop et al., 2000; McCusker et al., 2007). In contrast, when *cdc42-1* is inactivated, cells undergo a uniform arrest as very large unbudded cells (Adams et al., 1990). This indicates that buds and unbudded cells continue to grow when *cdc42-1* is inactivated. These observations suggest that slow depolarized growth takes place when the actin cytoskeleton is depolarized, in contrast to the effects of inactivating *cdk1-as1*. Second, if inhibition of *cdk1-as1* exerted its

effects via depolarization of the actin cytoskeleton, one should be able to detect significant numbers of vesicles in cells after inhibition of *cdk1-as1*. However, we detected few GFP-Sec4 marked vesicles when *cdk1-as1* was inhibited, whereas vesicles were detected in *cdc42-1* cells.

It may seem surprising that inhibition of *cdk1-as1* causes severe defects in trafficking of post-Golgi vesicles but does not cause severe defects in trafficking of several secretory cargoes. However, previous work showed that even quite strong blocks in exocytic trafficking such as those seen in *exo84-112*, *sec6-4*, *cdc42-6*, or *ypt31/32 Δ* can leave other trafficking pathways such as the CPY route intact and operational with normal kinetics (Jedd et al., 1997; Adamo et al., 2001; Zhang et al., 2005). Conversely, endocytic mutants such as *sla2 Δ* and *end4 Δ* are normal in CPY trafficking and invertase secretion (Raths et al., 1993; Mulholland et al., 1997). Similarly, invertase secretion has been reported to be normal in the endosome-to-plasma membrane recycling mutant *rcy1 Δ* (Wiederkehr et al., 2000).

We observed that sites of actin-dependent endocytosis form a ring that surrounds a central axis of exocytosis at the site of polarized growth, as suggested by previous studies that separately observed sites of endocytosis or exocytosis (Kilmartin and Adams, 1984; Amberg, 1998; Finger et al., 1998; Layton et al., 2011). Endocytic and exocytic compartments are also closely apposed in *Aspergillus nidulans* (Taheri-Talesh et al., 2008). Studies suggest that close coordination of endocytic uptake and recycling helps to optimize cell polarity (Valdez-Taubas and Pelham, 2003; Marco et al., 2007). The molecular mechanisms underlying the relative organization of endocytic and exocytic sites are poorly understood, but our observations here suggest that Cdk1 plays a role.

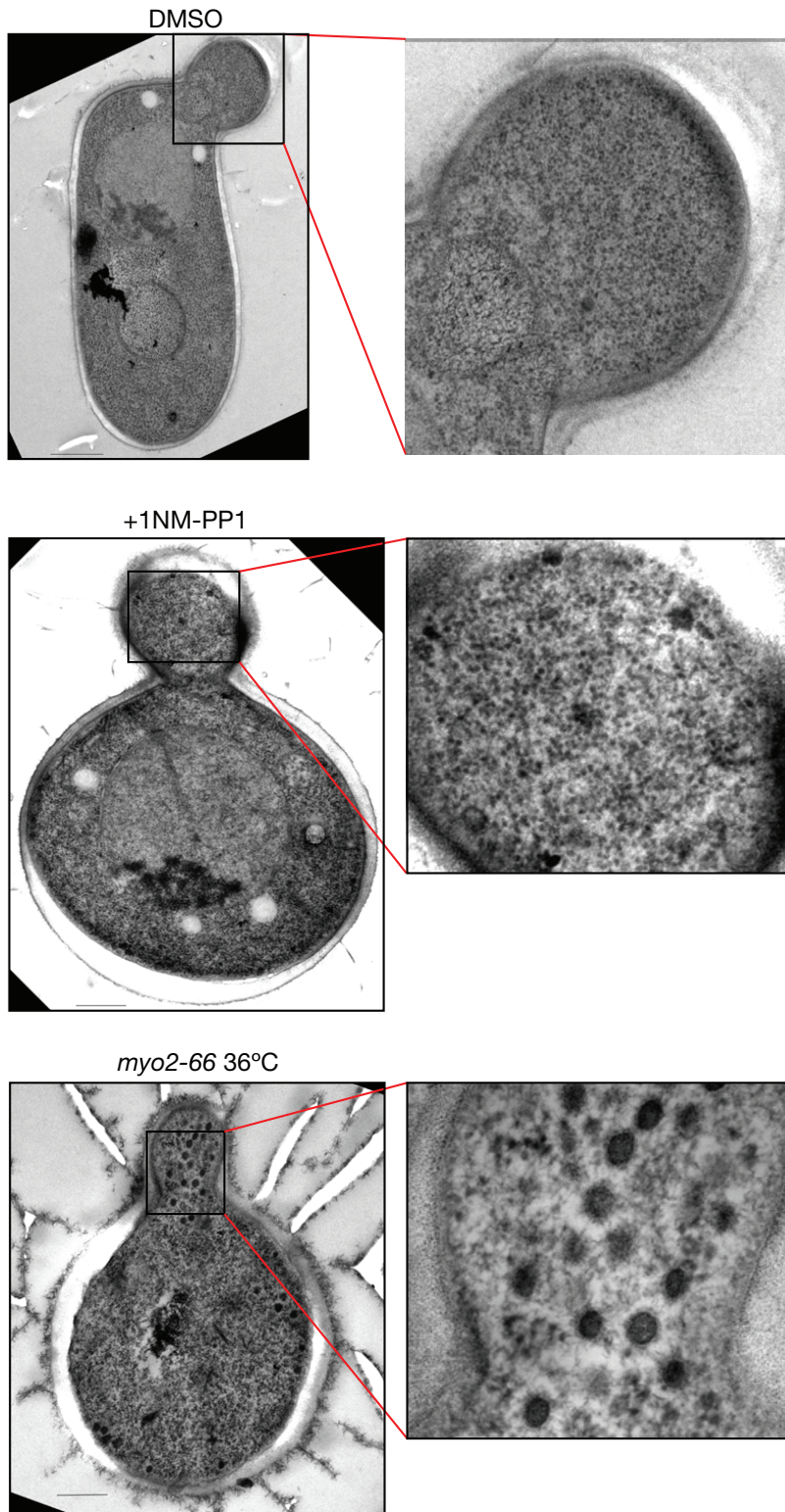


FIGURE 7: Accumulation of cytoplasmic vesicles after inactivation of *myo2-66* but not after *cdk1-as1* inhibition. Cells were grown to early-log phase and treated for 1 h with DMSO as a control, with 1NM-PP1 to inactivate *cdk1-as1*, or shifted to 36°C for 1 h to inactivate *myo2-66*. After rapid freezing, cells were freeze substituted and processed for transmission electron microscopy. Scale bar, 200 nm.

In summary, these observations suggest that Cdk1 plays a role in regulating membrane dynamics to coordinate membrane growth with cell cycle progression. Yeast cells are able to maintain the same

basic size and shape despite widely varying growth rates caused by changes in nutrient availability or other external stresses. Direct control of membrane dynamics by Cdk1 would offer an attractive model for linking membrane growth to cell cycle progression. Identification of the molecular mechanisms targeted by Cdk1 to control membrane dynamics will be an important focus for future work.

MATERIALS AND METHODS

Yeast strains and procedures

A list of the yeast strains used in this study is provided in Table 1. Tagging of open reading frames at the C-terminus was achieved by PCR-based homologous recombination at the endogenous gene locus. GFP-Sec4 was expressed from a CEN vector (pRS315) under the control of the *Sec4* promoter (Schott *et al.*, 2002). Unless stated, cells were grown in yeast extract/peptone/dextrose (ThermoFisher Scientific, Waltham, MA) or selective media supplemented with 50 μg/ml adenine sulfate (ICN Biomedicals, Irvine, CA) at 23°C.

Treatment of cells with inhibitors

In all experiments involving addition of inhibitors, cells were treated with 25 μM 1NM-PP1 (Calbiochem, La Jolla, CA) to inhibit *cdk1-as1* activity or 100 μM latrunculin-A to inhibit F-actin.

Centrifugal elutriation

A 1.3-l culture of cells was grown overnight to OD₆₀₀ 1.4. A synchronous population of unbudded cells was obtained by centrifugal elutriation. Cells were centrifuged at 2700 rpm and elutriated at 31 ml/min. Cells were released into fresh media and monitored for the synchronous formation of small buds, an indicator of the initiation of polarized growth. At bud formation, cells were treated with DMSO (Sigma-Aldrich, St. Louis, MO) or with inhibitors. Treated cells were incubated at 23°C for 1 h and then fixed in 3.7% formaldehyde (ThermoFisher Scientific) for 1 h.

Microscopy

Cells were grown to early logarithmic phase in selective media, treated with 1NM-PP1 for the times indicated, and attached to coverslips that had been coated with 1 mg/ml concanavalin-A (Sigma-Aldrich). Coverslips were then mounted onto glass slides using two pieces of double-sided tape. For single-section wide-field images (Figures 1, 2B, 3, and 5), cells were visualized using a Zeiss Axioskop II microscope with a Zeiss AxioCam HRm camera (Carl Zeiss, Jena, Germany). Photobleaching was minimized using

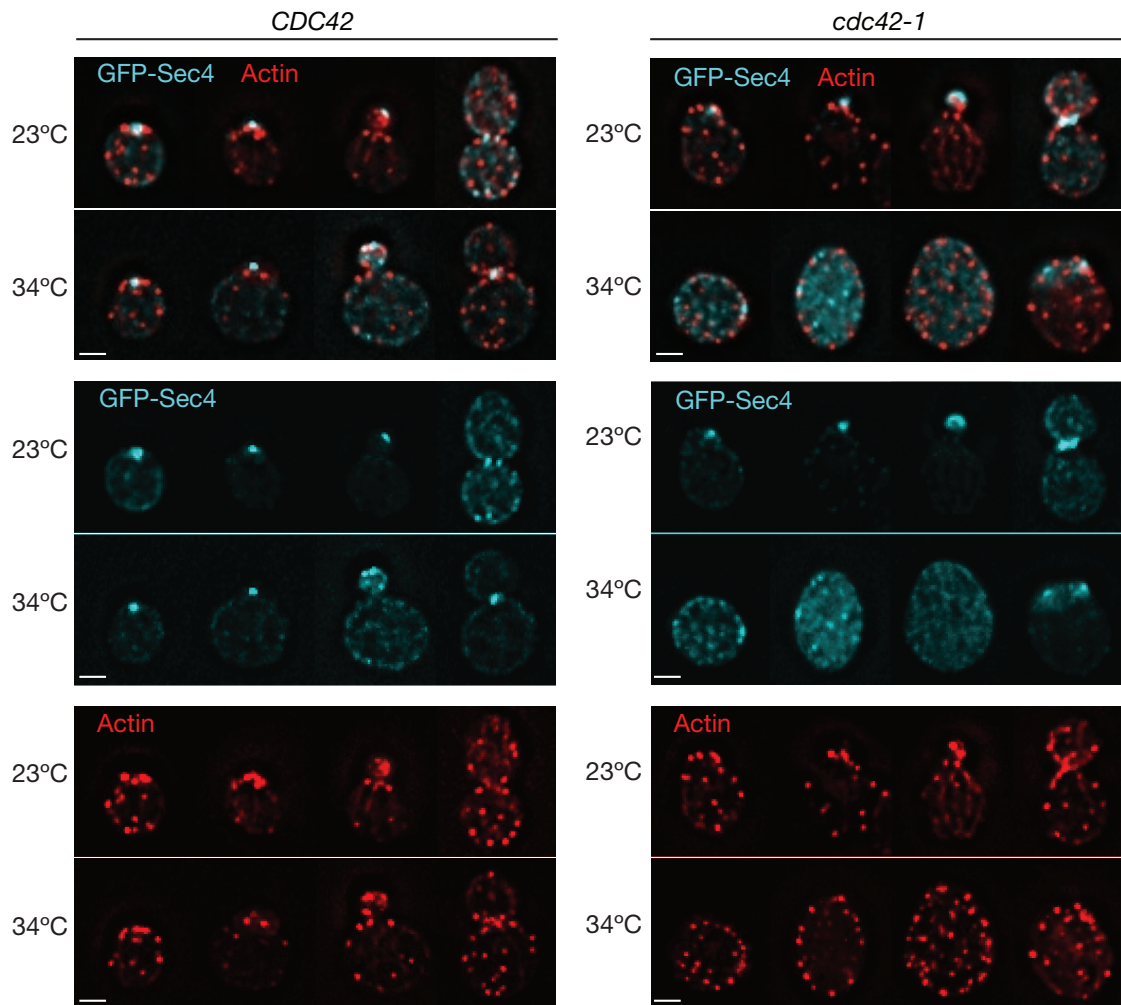


FIGURE 8: Accumulation of cytoplasmic GFP-Sec4 in *cdc42-1* mutant cells. Cells expressing GFP-Sec4 (cyan) were shifted to the temperature indicated and fixed after 3 h. The actin cytoskeleton (red) was stained with Alexa 546-phalloidin. Images show maximum projections of 15–20 deconvolved z-sections through different cells at distinct cell cycle stages. Shown are individual GFP-Sec4 and actin channels and the merge of the two signals. Scale bar, 2 μ m.

a Uniblitz VMMD1 external shutter driver (Uniblitz, Rochester, NY). A 100 \times (numerical aperture [NA] 1.3) Plan-Neofluar (Carl Zeiss) oil objective was used to visualize cells. Image acquisition was performed using Zeiss AxioVision software. Kymographs were generated using MetaMorph software (Molecular Devices, Sunnyvale, CA). Multiple z-sections shown in Figure 2A were acquired on a DMI600B inverted Leica fluorescent microscope (Leica, Wetzlar, Germany) equipped with a Hamamatsu ORCA C9100 EM-CCD camera (Hamamatsu Photonics, Hamamatsu, Japan) and a 100 \times (NA 1.4) Plan-Apochromat oil objective. From 15 to 20 0.2- μ m steps were acquired using Leica LASAF6000 software. Ten iterations of a blind deconvolution algorithm were run, using a refractive index of 1.5.

High-speed near-TIRFM was used to monitor GFP-Sec4 puncta in Figure 6. In near-TIRFM, the incidence angle of the laser with respect to the sample is reduced, generating a deeper evanescent field. This configuration was used to resolve puncta moving beneath the cell wall in budding yeast. The TIRFM system comprised an Axiovert 200M (Carl Zeiss) microscope chassis with a 100 \times (NA 1.46) Plan Apochromat oil objective with an additional 1.6 Optovar lens, an Evolve EM-CCD camera (Photometrics, Tucson, AZ) and a Dual View DV2 beam-splitter (Photometrics). Samples were illuminated

using acousto-optic tunable filter-controlled 488- and 561-nm laser lines coupled to a motorized TIRF slider (Carl Zeiss) via a single-mode fiber. The system was controlled by MetaMorph software. The data presented in Figure 6 were generated by acquiring images at 30-ms intervals and generating kymographs using MetaMorph.

Electron microscopy

Cells were pelleted, and the pellets were placed on the surface of a copper electron microscopy grid (400 mesh) that had been coated with Formvar. Each loop was quickly immersed in liquid propane precooled and maintained at -180°C using liquid nitrogen. The loops were then transferred to a precooled solution of 4% osmium tetroxide in dry acetone in a 1.8-ml polypropylene vial at -82°C for 72 h (substitution) and warmed gradually to room temperature, followed by three washes in dry acetone. Specimens were stained in the dark for 1 h in 1% uranyl acetate in acetone at 4°C . After an additional rinse in dry acetone, the samples were infiltrated progressively with araldite (epoxy resin; Fluka, Sigma-Aldrich). Ultrathin sections were contrasted with lead citrate and observed with a Hitachi 7650 electron microscope (Hitachi, Tokyo, Japan; Bordeaux Imaging Center, Electronic Microscopy Pole of the University of Bordeaux 2).

Name	Genotype	Reference
DK186	<i>MATa bar1 his3-11,15 leu2-3112 trp1-1 ura3-1 ade2-1 can1-100</i>	
DMY496	<i>MATa bar1 cdc28-as1^a</i>	Bishop et al. (2001)
DMY401	<i>MATa bar1 cdc28-as1 sla2Δ::kanMX6</i>	This study
DMY543	<i>MATa bar1 cdc28-as1 SEC2-GFP::HIS3MX6</i>	This study
DMY891	<i>MATa bar1 BGL2-6XHA::HIS3MX6</i>	This study
DMY894	<i>MATa bar1 cdc28-as1 BGL2-6XHA::HIS3MX6</i>	This study
DMY870	<i>MATa bar1 SUC2-3XHA::HIS3MX6</i>	This study
DMY872	<i>MATa bar1 cdc28-as1 SUC2-3XHA::HIS3MX6</i>	This study
DMY890	<i>MATa sec6-4 SUC2-3XHA::HIS3MX6</i>	This study

^aNote that the budding yeast *CDC28* gene encodes Cdk1. We refer to cyclin-dependent kinase 1 as Cdk1 throughout this article.

TABLE 1: Strains used in this work.

Assays for secretion and endocytosis

Invertase (*Suc2*) secretion was monitored using a 3xHA-tagged version of the protein, as used previously (Gillingham et al., 2006). Cells were grown to early logarithmic phase in yeast extract/peptone/dextrose (YPD) and then shifted to yeast extract/peptone (YEP) media containing 0.1% dextrose and 1NM-PP1 or DMSO (control) for 1 h to induce invertase secretion. *sec6-4* cells were resuspended in YEP + 0.1% dextrose and then immediately shifted to 34°C for 1 h. At the end of the experiment, NaN₃ and NaF were added to 10 mM, and cells were incubated on ice for 10 min. Cells were then rinsed in wash buffer (20 mM Tris-HCl, pH 7.5, 10 mM NaN₃, 10 mM NaF). We removed 1.5 OD₆₀₀ of cells and resuspended them in 150 μl of spheroplast buffer (50 mM Tris-HCl, pH 7.5, 1.4 M sorbitol, 10 mM NaN₃, 10 mM NaF, 30 mM 2-mercaptoethanol, 0.2 mg ml⁻¹ Zymolyase 100T; Seikagaku, Tokyo, Japan) and incubated at 37°C for 20 min to digest the cell wall. All subsequent steps were carried out at 4°C. Spheroplasts were pelleted by centrifugation at 2000 × g for 3 min. A 100-μl supernatant (external secreted fraction) was removed and boiled in 4× SDS-PAGE sample buffer. The spheroplast pellet was washed twice in spheroplast wash buffer (50 mM Tris-HCl, pH 7.5, 1.4 M sorbitol, 10 mM NaF, 10 mM NaN₃). Spheroplasts were resuspended in 120 μl of lysis buffer (20 mM Tris-HCl, pH 7.5, 100 mM NaCl, 2 mM MgCl₂, 0.5% Triton-X100, 2 mM phenylmethylsulfonyl fluoride [PMSF], 1 μg/ml leupeptin, 1 μg/ml pepstatin-A, 1 μg/ml chymostatin), vortexed for 30 s, and then centrifuged at 82 × g for 5 min. A 100-μl supernatant (internal fraction) was boiled in 1× SDS-PAGE sample buffer. Samples were resolved using 7.5% SDS-PAGE, blotted, and probed with anti-HA polyclonal antisera. Internal and external Bgl2 levels were measured in the same manner, except that cells were maintained in YPD media, and Bgl2 was resolved using 12.5% SDS-PAGE. The cytoplasmic protein Nap1 was not detected in the extracellular fraction, indicating that cells were not overspheroplasted (unpublished data).

Endocytosis was assayed by pulse chasing the lipophilic dye FM4-64 (Invitrogen, Carlsbad, CA) through the endocytic pathway. Early-logarithmic-phase cells were treated with 25 μM 1NM-PP1 for 1 h at 23°C and placed on ice for 5 min to block endocytosis, and FM4-64 was then added to 16 μM for 15 min (on ice). Cells were then washed into fresh YPD media at 23°C containing 25 μM 1NM-PP1 to initiate the endocytic chase and imaged at the indicated times.

CPY transport assays

An overnight culture of logarithmic-phase cells was resuspended in minimal media lacking methionine and containing 2 mg/ml bovine serum albumin (Sigma-Aldrich). After 1 h of treatment with 1NM-PP1, or DMSO as a control, cells were adjusted to a concentration of 1 OD₆₀₀/ml. Cells were incubated with 25 μCi ³⁵S-methionine (Amersham-Pharmacia Biotech, GE Healthcare Bio-Sciences, Piscataway, NJ) per OD₆₀₀ for 10 min (pulse), and the chase was then initiated by the addition of 10× chase mix (20% glucose, 50 mM methionine) to a final concentration of 1×. At the times indicated, 1 OD₆₀₀ of cells was centrifuged and rapidly frozen in liquid nitrogen.

To immunoprecipitate CPY, metabolically labeled cells were resuspended in 75 μl of lysis buffer (1% SDS, 8 M urea, 2 mM PMSF, 1 μg/ml leupeptin, 1 μg/ml pepstatin-A, 1 μg/ml chymostatin) and lysed by glass bead agitation for 1 min, 30 s in a cell homogenizer (BioSpec, Bartlesville, OK). Fresh buffer was added to give a final lysis buffer composition (10 mM Tris-HCl, pH 8.0, 0.1% Tween-20, 2 mM EDTA, 0.05% SDS, 40 mM urea, 100 mM NaCl). Insoluble debris was removed after centrifugation at 16,000 × g for 15 min. A 2-μl amount of anti-CPY was added to each tube, and immunoprecipitations were carried out for 1 h at room temperature. We added 20 μl of protein-A agarose (Bio-Rad, Hercules, CA) to each tube for 1 h and then washed the samples four times in 1.5 ml of wash buffer (10 mM Tris-HCl pH 8.0, 0.1% SDS, 0.1% Tween-20, 2 mM EDTA). Immunoprecipitates were resolved by SDS-PAGE (7.5% acrylamide) and analyzed using a PhosphorImager (Molecular Dynamics, Sunnyvale, CA).

ACKNOWLEDGMENTS

We gratefully acknowledge the expertise of Benedicte Salin in conducting the electron microscopy experiments presented in Figure 7. We also thank Robert Arkowitz, Patrick Brennwald, Wei Guo, David Drubin, Ruth Collins, Marcus Babst, Randy Schekman, and Phil Crews for reagents and/or advice. Finally, we thank members of the Kellogg lab for helpful discussions. This work was funded by National Institutes of Health Grant GM053959-10 to D.K. Work in D.M.'s lab is funded by FP7 Marie Curie Grant IRG249298/Growth and Division, Agence Nationale de la Recherche Grant 2010 JCJC 1210 01, Fondation pour la Recherche Medicale Grant (INE20100518678), the Centre National de la Recherche Scientifique, Université de Bordeaux 2, and Conseil Régional d'Aquitaine Volet Recherche 20091301015.

REFERENCES

- Adamo JE, Moskow JJ, Gladfelter AS, Viterbo D, Lew DJ, Brennwald PJ (2001). Yeast Cdc42 functions at a late step in exocytosis, specifically during polarized growth of the emerging bud. *J Cell Biol* 155, 581–592.
- Adams AE, Johnson DI, Longnecker RM, Sloat BF, Pringle JR (1990). CDC42 and CDC43, two additional genes involved in budding and the establishment of cell polarity in the yeast *Saccharomyces cerevisiae*. *J Cell Biol* 111, 131–142.
- Amberg DC (1998). Three-dimensional imaging of the yeast actin cytoskeleton through the budding cell cycle. *Mol Biol Cell* 9, 3259–3262.
- Ayscough KR, Stryker J, Pokala N, Sanders M, Crews P, Drubin DG (1997). High rates of actin filament turnover in budding yeast and roles for actin in establishment and maintenance of cell polarity revealed using the actin inhibitor latrunculin-A. *J Cell Biol* 137, 399–416.
- Bishop AC, Buzko O, Shokat KM (2001). Magic bullets for protein kinases. *Trends Cell Biol* 11, 167–172.
- Bishop AC et al. (2000). A chemical switch for inhibitor-sensitive alleles of any protein kinase. *Nature* 407, 395–401.
- Culotti J, Hartwell LH (1971). Genetic control of the cell division cycle in yeast. 3. Seven genes controlling nuclear division. *Exp Cell Res* 67, 389–401.
- Eitzen G, Thorngren N, Wickner W (2001). Rho1p and Cdc42p act after Ypt7p to regulate vacuole docking. *EMBO J* 20, 5650–5656.
- Evangelista M, Blundell K, Longtine MS, Chow CJ, Adames N, Pringle JR, Peter M, Boone C (1997). Bni1p, a yeast formin linking cdc42p and the actin cytoskeleton during polarized morphogenesis. *Science* 276, 118–122.

- Finger FP, Hughes TE, Novick P (1998). Sec3p is a spatial landmark for polarized secretion in budding yeast. *Cell* 92, 559–571.
- Gillingham AK, Whyte JR, Panic B, Munro S (2006). Mon2, a relative of large Arf exchange factors, recruits Dop1 to the Golgi apparatus. *J Biol Chem* 281, 2273–2280.
- Govindan B, Bowser R, Novick P (1995). The role of Myo2, a yeast class V myosin, in vesicular transport. *J Cell Biol* 128, 1055–1068.
- Guo W, Tamanoi F, Novick P (2001). Spatial regulation of the exocyst complex by Rho1 GTPase. *Nat Cell Biol* 3, 353–360.
- Harsay E, Schekman R (2002). A subset of yeast vacuolar protein sorting mutants is blocked in one branch of the exocytic pathway. *J Cell Biol* 156, 271–285.
- Hasilik A, Tanner W (1978). Biosynthesis of the vacuolar yeast glycoprotein carboxypeptidase Y. Conversion of precursor into the enzyme. *Eur J Biochem* 85, 599–608.
- Holt LJ, Tuch BB, Villen J, Johnson AD, Gygi SP, Morgan DO (2009). Global analysis of Cdk1 substrate phosphorylation sites provides insights into evolution. *Science* 325, 1682–1686.
- Holtzman DA, Yang S, Drubin DG (1993). Synthetic-lethal interactions identify two novel genes, SLA1 and SLA2, that control membrane cytoskeleton assembly in *Saccharomyces cerevisiae*. *J Cell Biol* 122, 635–644.
- Isgandarova S, Jones L, Forsberg D, Loncar A, Dawson J, Tedrick K, Eitzen G (2007). Stimulation of actin polymerization by vacuoles via Cdc42p-dependent signaling. *J Biol Chem* 282, 30466–30475.
- Jedd G, Mulholland J, Segev N (1997). Two new Ypt GTPases are required for exit from the yeast *trans*-Golgi compartment. *J Cell Biol* 137, 563–580.
- Johnston GC, Prendergast JA, Singer RA (1991). The *Saccharomyces cerevisiae* MYO2 gene encodes an essential myosin for vectorial transport of vesicles. *J Cell Biol* 113, 539–551.
- Kilmartin J, Adams AEM (1984). Structural rearrangements of tubulin and actin during the cell cycle of the yeast *Saccharomyces*. *J Cell Biol* 98, 922–933.
- Kim K, Galletta BJ, Schmidt KO, Chang FS, Blumer KJ, Cooper JA (2006). Actin-based motility during endocytosis in budding yeast. *Mol Biol Cell* 17, 1354–1363.
- Knaus M, Pelli-Gulli MP, van Drogen F, Springer S, Jaquenoud M, Peter M (2007). Phosphorylation of Bem2p and Bem3p may contribute to local activation of Cdc42p at bud emergence. *EMBO J* 26, 4501–4513.
- Kono K, Nogami S, Abe M, Nishizawa M, Morishita S, Pellman D, Ohya Y (2008). G1/S cyclin-dependent kinase regulates small GTPase Rho1p through phosphorylation of RhoGEF Tus1p in *Saccharomyces cerevisiae*. *Mol Biol Cell* 19, 1763–1771.
- Kroschewski R, Hall A, Mellman I (1999). Cdc42 controls secretory and endocytic transport to the basolateral plasma membrane of MDCK cells. *Nat Cell Biol* 1, 8–13.
- Kubler E, Riezman H (1993). Actin and fimbrin are required for the internalization step of endocytosis in yeast. *EMBO J* 12, 2855–2862.
- Layton AT, Savage NS, Howell AS, Carroll SY, Drubin DG, Lew DJ (2011). Modeling vesicle traffic reveals unexpected consequences for Cdc42p-mediated polarity establishment. *Curr Biol* 21, 184–194.
- Lew DJ, Reed SI (1993). Morphogenesis in the yeast cell cycle: regulation by Cdc28 and cyclins. *J Cell Biol* 120, 1305–1320.
- Marco E, Wedlich-Soldner R, Li R, Altschuler SJ, Wu LF (2007). Endocytosis optimizes the dynamic localization of membrane proteins that regulate cortical polarity. *Cell* 129, 411–422.
- McCusker D, Denison C, Anderson S, Egelhofer TA, Yates JR 3rd, Gygi SP, Kellogg DR (2007). Cdk1 coordinates cell-surface growth with the cell cycle. *Nat Cell Biol* 9, 506–515.
- Moffat J, Andrews B (2004). Late-G1 cyclin-CDK activity is essential for control of cell morphogenesis in budding yeast. *Nat Cell Biol* 6, 59–66.
- Moseley JB, Nurse P (2009). Cdk1 and cell morphology: connections and directions. *Curr Opin Cell Biol* 21, 82–88.
- Mulholland J, Wesp A, Riezman H, Botstein D (1997). Yeast actin cytoskeleton mutants accumulate a new class of Golgi-derived secretory vesicle. *Mol Biol Cell* 8, 1481–1499.
- Murray JM, Johnson DI (2001). The Cdc42p GTPase and its regulators Nrf1p and Scd1p are involved in endocytic trafficking in the fission yeast *Schizosaccharomyces pombe*. *J Biol Chem* 276, 3004–3009.
- Nasmyth K (2001). A prize for proliferation. *Cell* 107, 689–701.
- Nern A, Arkowitz RA (2000). Nucleocytoplasmic shuttling of the Cdc42p exchange factor Cdc24p. *J Cell Biol* 148, 1115–1122.
- Novick P, Botstein D (1985). Phenotypic analysis of temperature-sensitive yeast actin mutants. *Cell* 40, 405–416.
- Osman MA, Cerione RA (1998). Iqg1p, a yeast homologue of the mammalian IQGAPs, mediates cdc42p effects on the actin cytoskeleton. *J Cell Biol* 142, 443–455.
- Raths S, Rohrer J, Crausaz F, Riezman H (1993). end3 and end4: two mutants defective in receptor-mediated and fluid-phase endocytosis in *Saccharomyces cerevisiae*. *J Cell Biol* 120, 55–65.
- Roberts CJ, Nothwehr SF, Stevens TH (1992). Membrane protein sorting in the yeast secretory pathway: evidence that the vacuole may be the default compartment. *J Cell Biol* 119, 69–83.
- Schott D, Ho J, Pruyne D, Bretscher A (1999). The COOH-terminal domain of Myo2p, a yeast myosin V, has a direct role in secretory vesicle targeting. *J Cell Biol* 147, 791–808.
- Schott DH, Collins RN, Bretscher A (2002). Secretory vesicle transport velocity in living cells depends on the myosin-V lever arm length. *J Cell Biol* 156, 35–39.
- Shimada Y, Gulli MP, Peter M (2000). Nuclear sequestration of the exchange factor Cdc24 by Far1 regulates cell polarity during yeast mating. *Nat Cell Biol* 2, 117–124.
- Shuster CB, Burgess DR (2002). Targeted new membrane addition in the cleavage furrow is a late, separate event in cytokinesis. *Proc Natl Acad Sci USA* 99, 3633–3638.
- Sopko R, Huang D, Smith JC, Figeys D, Andrews BJ (2007). Activation of the Cdc42p GTPase by cyclin-dependent protein kinases in budding yeast. *EMBO J* 26, 4487–4500.
- Stevens T, Esmon B, Schekman R (1982). Early stages in the yeast secretory pathway are required for transport of carboxypeptidase Y to the vacuole. *Cell* 30, 439–448.
- Taheri-Talesh N, Horio T, Araujo-Bazan L, Dou X, Espeso EA, Penalva MA, Osmani SA, Oakley BR (2008). The tip growth apparatus of *Aspergillus nidulans*. *Mol Biol Cell* 19, 1439–1449.
- Takizawa PA, DeRisi JL, Wilhelm JE, Vale RD (2000). Plasma membrane compartmentalization in yeast by messenger RNA transport and a septin diffusion barrier. *Science* 290, 341–344.
- TerBush DR, Maurice T, Roth D, Novick P (1996). The Exocyst is a multi-protein complex required for exocytosis in *Saccharomyces cerevisiae*. *EMBO J* 15, 6483–6494.
- TerBush DR, Novick P (1995). Sec6, Sec8, and Sec15 are components of a multisubunit complex which localizes to small bud tips in *Saccharomyces cerevisiae*. *J Cell Biol* 130, 299–312.
- Valdez-Taubas J, Pelham HR (2003). Slow diffusion of proteins in the yeast plasma membrane allows polarity to be maintained by endocytic cycling. *Curr Biol* 13, 1636–1640.
- VerPlank L, Li R (2005). Cell cycle-regulated trafficking of Chs2 controls actomyosin ring stability during cytokinesis. *Mol Biol Cell* 16, 2529–2543.
- Vida TA, Emr SD (1995). A new vital stain for visualizing vacuolar membrane dynamics and endocytosis in yeast. *J Cell Biol* 128, 779–792.
- Wiederkehr A, Avaro S, Prescianotto-Baschong C, Haguenaer-Tsapis R, Riezman H (2000). The F-box protein Rcy1p is involved in endocytic membrane traffic and recycling out of an early endosome in *Saccharomyces cerevisiae*. *J Cell Biol* 149, 397–410.
- Wiederkehr A, Du Y, Pypaert M, Ferro-Novick S, Novick P (2003). Sec3p is needed for the spatial regulation of secretion and for the inheritance of the cortical endoplasmic reticulum. *Mol Biol Cell* 14, 4770–4782.
- Wilcox CA, Redding K, Wright R, Fuller RS (1992). Mutation of a tyrosine localization signal in the cytosolic tail of yeast Kex2 protease disrupts Golgi retention and results in default transport to the vacuole. *Mol Biol Cell* 3, 1353–1371.
- Wu H, Rossi G, Brennwald P (2008). The ghost in the machine: small GTPases as spatial regulators of exocytosis. *Trends Cell Biol* 18, 397–404.
- Zhang X, Orlando K, He B, Xi F, Zhang J, Zajac A, Guo W (2008). Membrane association and functional regulation of Sec3 by phospholipids and Cdc42. *J Cell Biol* 180, 145–158.
- Zhang X, Zajac A, Zhang J, Wang P, Li M, Murray J, TerBush D, Guo W (2005). The critical role of Exo84p in the organization and polarized localization of the exocyst complex. *J Biol Chem* 280, 20356–20364.